Synthesis and Characterization of a 1:6 Au−CdSe Nanocomposite

Scott L. Cumberland, Mia G. Berrettini, Artjay Javier, and Geoffrey F. Strouse*

Department of Chemistry and Biochemistry, University of California, Santa Barbara, California 93106

Received June 15, 2001. Revised Manuscript Received December 23, 2002

Development of synthetic strategies that allow the formation of controlled 3-dimensional architectures composed of discrete ensembles of nanoparticles is a challenging goal. We present a synthetic strategy that allows the preparation of a macroscopic 3-D metal−semiconductor assemblage composed of 6.0-nm Au and 6.0-nm CdSe nanoparticles cross-linked by a bifunctional organic spacer. Optical absorption and electron microscopy imaging, coupled to electron diffraction and energy-dispersive X-ray analysis, indicate a 1:6 Au−CdSe composite that appears to be uniform over a micrometer scale. The 1:6 structure is believed to be a close-packed structure which arises from a combination of soft-sphere packing forces due to van der Waals and steric forces, and thermodynamic forces due to an acid/base controlled selective interaction of the organic headgroup moieties with the nanoparticle surfaces.

Introduction

Developing novel approaches for assembling nanoscale materials into interconnected, organized lattices has formed a cornerstone of research in nano-electronics, catalysts, and formation of unique hybrid materials. Synthetic techniques allow uniform nanomaterials to be prepared having surface passivating ligands that can be used to control nanoparticle organization in 2- and 3-dimensional architectures.[1−10] In analogy to exchange reactions on self-assembled monolayers (SAM), the nanomaterial surface ligands can be exchanged allowing the incorporation of a ligand possessing a terminal functionality capable of selective interactions.[11−16] This permits the terminal functionality to be used in the assembly of nanomaterials through forces such as hydrogen bonding, electrostatics, or hydrophobic interactions. Several methodologies for component assemblies of nanoparticles have been employed to generate unique inorganic−organic composites. Single-component assemblies can be generated using Langmuir−Blodgett (L−B) techniques, polyeletrolyte assembly, evaporative self-assembly, self-assembled multilayers via ligand templating, and dendrimer-based approaches.[2,9,18−31] Biomaterial assemblies have been demonstrated using both thiol-modified DNA and cysteine-rich proteins as building blocks for the inorganic−organic composite.[32−37] Recently, electrostatic interactions have been utilized

* To whom correspondence should be addressed. Phone: 805-893-5326. Fax: 805-893-4120. E-mail: strouse@chem.ucsb.edu.

(1) Ahmadi, T. S.; Wang, Z. L.; Green, T. C.; Henglein, A.; El-Sayed, M. A. *Science* **1996**, *272*, 1924.
(2) Danek, M.; Jensen, K. F.; Murray, C. B.; Bawendi, M. G. *J. Cryst. Growth* **1994**, *145*, 714.
(3) Cumberland, S. L.; Hanif, K. A.; Khitrov, G. A.; Javier, A.; Strouse, G. F.; Woessner, S. M.; Yun, C. S. *Chem. Mater.* **2002**, *14*, 1576−1584.
(4) Muhlpfordt, H. *Experientia* **1982**, *38*, 1127.
(5) Murray, C. B.; Norris, D. J.; Bawendi, M. G. *J. Am. Chem. Soc.* **1993**, *115*, 8706.
(6) Murray, C. B.; Nirmal, M.; Norris, D. J.; Bawendi, M. G. *Z. Phys. D* **1993**, *26*, S231.
(7) Murthy, S.; Bigioni, T. P.; Wang, Z. L.; Khoury, J. T.; Whetten, R. L. *Mater. Lett.* **1997**, *30*, 321.
(8) Slot, J. W.; Geuze, H. J. *Eur. J. Cell Bio.* **1985**, *38*, 87.
(9) Sun, S. H.; Murray, C. B. *J. Appl. Phys.* **1999**, *85*, 4325.
(10) Whetten, R. L.; Khoury, J. T.; Alvarez, M. M.; Murthy, S.; Vezmar, I.; Wang, Z. L.; Stephens, P. W.; Cleveland, C. L.; Luedtke, W. D.; Landman, U. *Adv. Mater.* **1996**, *8*, 428.
(11) Chen, S. W.; Murray, R. W. *J. Phys. Chem. B* **1999**, *103*, 9996.
(12) Warner, M. G.; Reed, S. M.; Hutchison, J. E. *Chem. Mater.* **2000**, *12*, 3316.
(13) Zamborini, F. P.; Gross, S. M.; Murray, R. W. *Langmuir* **2001**, *17*, 481.
(14) Schreiber, F. *Prog. Surf. Sci.* **2000**, *65*, 151.
(15) Xia, Y.; Kim, E.; Whitesides, G. M. *J. Electrochem. Soc.* **1996**, *143*, 1070.
(16) Chen, S.; Kimura, K. *Chem. Lett.* **1999**, *3*, 233.
(17) Harfenist, S. A.; Wang, Z. L.; Whetten, R. L.; Vezmar, I.; Alvarez, M. M. *Adv. Mater.* **1997**, *9*, 817.
(18) Mattoussi, H.; Mauro, J. M.; Goldman, E. R.; Anderson, G. P.; Sundar, V. C.; Mikulec, F. V.; Bawendi, M. G. *J. Am. Chem. Soc.* **2000**, *122* (49), 12142−12150.
(19) Sun, S. H.; Murray, C. B.; Weller, D.; Folks, L.; Moser, A. *Science* **2000**, *287*, 1989.
(20) Wang, Z. L. *Adv. Mater.* **1998**, *10*, 13.
(21) Korgel, B. A.; Fullam, S.; Connolly, S.; Fitzmaurice, D. *J. Phys. Chem. B* **1998**, *102*, 8379.
(22) Murray, C. B.; Kagan, C. R.; Bawendi, M. G. *Annu. Rev. Mater. Sci.* **2000**, *30*, 545.
(23) Danek, M.; Jensen, K. F.; Murray, C. B.; Bawendi, M. G. *Appl. Phys. Lett.* **1994**, *65*, 2795.
(24) Collier, C. P.; Vossmeyer, T.; Heath, J. R. *Annu. Rev. Phys. Chem.* **1998**, *49*, 371−404.
(25) Cassagneau, T.; Mallouk, T.; Fendler, J. *J. Am. Chem. Soc.* **1998**, *120* (31), 7848−7859.
(26) Cassagneau, T.; Fendler, J. *J. Phys. Chem. B* **1999**, *103* (11), 1789−1793.
(27) Brittain, S.; Paul, K.; Zhao, X. M.; Whitesides, G. *Phys. World* **1998**, *11*, 31.
(28) Black, C. T.; Murray, C. B.; Sandstrom, R. L.; Sun, S. H. *Science* **2000**, *290*, 1131.
(29) Whetten, R. L.; Shafigullin, M. N.; Khoury, J. T.; Schaaff, T. G.; Vezmar, I.; Alvarez, M. M.; Wilkinson, A. *Acc. Chem. Res.* **1999**, *32*, 397.
(30) Musick, M. D.; Keating, C. D.; Lyon, L. A.; Botsko, S. L.; Pena, D. J.; Holliway, W. D.; McEvoy, T. M.; Richardson, J. N.; Natan, M. J. *Chem. Mater.* **2000**, *12*, 2869.
(31) Dabbousi, B. O.; Murray, C. B.; Rubner, M. F.; Bawendi, M. G. *Chem. Mater.* **1994**, *6*, 216.

10.1021/cm010588o CCC: $25.00
Published on Web 01/30/2003

to generate a 1:1 composite of Au and CdS, yielding a surprisingly ordered array.[38] Studies of these inorganic−organic structures suggest a surprising level of connectivity exists between the individual nano-components indicating controlled organization may be beneficial in future device applications.[17,38−44]

With the exception of the electrostatic or multilayer assembly approaches, 3-dimensional assemblies composed of two individual components are rarely observed, due to an inherent propensity for phase segregation of the individual nanomaterial components.[21,45] The propensity for phase segregation can be readily understood in analogy to micelle models for soft-sphere packing forces, where core interactions between individual nanomaterials are dictated by the polarizability of the nanomaterial (van der Waals interactions) and the sterics of the passivating layer on the nanomaterial surface. Phase segregation is surmountable by controlling assembly with a headgroup coordination event, rather than relying on van der Waals forces or minimum packing architectures. This results in a 3-D assembly that is governed by the nature of headgroup binding and the strength of the nanomaterial headgroup interaction rather than entirely by soft-packing forces.

We report the formation of 3-dimensional assemblies consisting of a Au−ligand−CdSe interconnecting framework that yields a 1:6 (Au−CdSe) close-packed architecture. The final order and rate of formation of the assembly is pH controlled (pH 4−6) via an acid/base equilibria arising from proton exchange between the R-NH_3^+ group of 2-aminoethanethiol passivated CdSe and the surface groups stabilizing the Au nanomaterial. Analysis of selected area electron diffraction (SAED) patterns in the TEM demonstrates that the 3-dimensional assembly exhibits a surprising degree of regularity, with an observed 1:6 mole ratio of Au to CdSe over multiple 500 × 500 nm regions of an isolated micrometer-sized fragment of the synthesized 3-D composite.

Experimental Section

Optical Measurements. FT-IR analysis was conducted using pressed KBr pellets on a Perkin-Elmer Spectrum GX FT-IR between 370 and 7000 cm^{-1} with a resolution of 4 cm^{-1}.

UV/Vis spectra were recorded at RT using an Ocean Optics S2000 CCD spectrometer (resolution 0.3 nm) either in H_2O for individual particles, or in a KBR pellet for solid-phase assemblies of Au−CdSe. The optical absorption of the KBr pellet containing 2−5 mg of the Au−CdSe composite was fit using a weighted combination of the solution phase 6.0-nm amino-ethanethiol (AET)-capped CdSe and 6.0-nm citrate-capped Au absorption spectra and extinction coefficients, as well as the inclusion of a scattering profile for the KBr pellet absorbance. Wavelength-dependent extinction functions, $\epsilon(\lambda)$, were extracted using published values for CdSe and Au.[46,47] In addition, the Au SPR bandwidth and energy were allowed to fit as a variable parameter to account for changes in the SPR band arising from changes in the local dielectric constant occurring in the assembly. Assuming electronically noninteracting species, this allows the linear absorbance spectrum to be fit as a linear combination of the constituents:

$$A_{\text{Composite}}(\lambda) = A_{\text{CdSe}}(\lambda) + A_{\text{Au}}(\lambda) + f_{\text{scat}}(\lambda) \qquad (1)$$

In the KBr pellet an additional term to account for energy-dependent light scattering effects ($f_{\text{scat}}(\lambda)$) was included. The scattering profile from a KBr absorbance spectrum was fit to the power law $f_{\text{scat}}(\lambda) = f(0) + m\,\lambda^{-n}$, where m, n, and $f(0)$ are fitting parameters. An empirical fit was obtained and was subsequently used to fit the absorbance spectrum of the composite.

Atomic absorption (AA) measurements of the composites were performed on a Varian Techtron flame AA instrument with the absorbance of gold taken at 267.6 nm and the absorbance of cadmium taken at 326.1 nm using an oxy-acetylene flame. Calibration standards containing Au and CdSe were prepared by High Purity Standards, Inc. to generate a linear calibration curve within the concentration limits of the assembly.

Emission measurements were performed on a CCD-based instrument utilizing the 458.0 nm Ar^+ ion laser line for excitation (power < 2 mW) and dispersion on a 0.5-M spectrometer. Laser line rejection was accomplished by use of a 458.0-nm holographic notch filter (Kaiser Optical).

Electron Microscopy. Transmission electron microscopy (TEM) measurements were conducted on a JEOL 2000 microscope operated at 200 kV in bright field mode using 400 mesh Ni or Cu grids coated with a ∼5-nm layer of holey carbon (SPI). Grids of individual CdSe and Au particles were prepared by dissolving them in water and using standard drop-cast techniques with slow evaporation, over 6−12 h. TEM images of the 3-D assembly were prepared by grinding the isolated micrometer-length black particulate material to generate smaller fragments for electron microscopy imaging. The ground materials were dispersed on a carbon grid for TEM measurements or on either a carbon or a Si wafer for SEM measurements by typical drop-cast methods. SAED analysis in the TEM was achieved at a magnification of 50 000 with a camera length of 83 cm. Scanning electron microscopy (SEM) images at 3 kV in backscattering mode were obtained on uncoated samples using a JEOL 6300 FE-SEM instrument with EDS and CL capabilities. Elemental mapping over 500 × 500 nm regions of the micrometer-scale composite was accomplished using a LYNX collector with Inca software from Oxford instruments attached to the SEM. The energy-dispersive X-ray analysis (EDX) was measured over 4−6 areas imaging a 500 × 500 nm region of the composite. The resolution in backscattrering imaging is 3.0 nm at 3 kV. The EDX intensities were calibrated to copper powder using JEOL instrumental protocols.

NMR Spectroscopy. ^{13}C NMR analyses of CdSe-AET and unbound AET were obtained on a Bruker 500 MHz Avance with a HX double resonance probe (D_2O, 25 °C). ^{13}C NMR analysis of HDA and CdSe−HDA in supplemental information was obtained on a Varian 500 MHz Unity Inova with a Nalorac 10 mm dual broadband probe ($CDCl_3$, 25 °C).

(32) Mucic, R. C.; Storhoff, J. J.; Mirkin, C. A.; Letsinger, R. L. *J. Am. Chem. Soc.* **1998**, *120*, 12674.
(33) Mitchell, G. P.; Mirkin, C. A.; Letsinger, R. L. *J. Am. Chem. Soc.* **1999**, *121*, 8122.
(34) Park, S. J.; Lazarides, A. A.; Mirkin, C. A.; Brazis, P. W.; Kannewurf, C. R.; Letsinger, R. L. *Angew. Chem., Int. Ed.* **2000**, *39*, 3845.
(35) Storhoff, J. J.; Mirkin, C. A. *Chem. Rev.* **1999**, *99*, 1849.
(36) Loweth, C. J.; Caldwell, W. B.; Peng, X. G.; Alivisatos, A. P.; Schultz, P. G. *Angew. Chem., Int. Ed.* **1999**, *38*, 1808.
(37) Alivisatos, A. P.; Johnsson, K. P.; Peng, X. G.; Wilson, T. E.; Loweth, C. J.; Bruchez, M. P.; Schultz, P. G. *Nature* **1996**, *382*, 609.
(38) Kolny, J.; Kornowski, A.; Weller, H. *Nano Lett.* **2002**, *2*, 361−364.
(39) Ginger, D. S.; Greenham, N. C. *J. Appl. Phys.* **2000**, *87*, 1361.
(40) Ginger, D. S.; Greenham, N. C. *Phys. Rev. B* **1999**, *59*, 10622.
(41) Takagahara, T. *J. Lumin.* **1996**, *70*, 129.
(42) Kagan, C. R.; Murray, C. B.; Nirmal, M.; Bawendi, M. G. *Phys. Rev. Lett.* **1996**, *76*, 1517.
(43) Rosenberg, R.; Murray, C. B. *Annu. Rev. Mater. Sci.* **2000**, *30*, XII.
(44) Kiely, C. J.; Fink, J.; Zheng, J. G.; Brust, M.; Bethell, D.; Schiffrin, D. J. *Adv. Mater.* **2000**, *12*, 640.
(45) Ohara, P. C.; Leff, D. V.; Heath, J. R.; Gelbart, W. M. *Phys. Rev. Lett.* **1995**, *75*, 3466.
(46) Schmelz, O.; Mews, A.; Basche, T.; Herrmann, A.; Mullen, K. *Langmuir* **2001**, *17* (9), 2861−2865.
(47) Cumberland, S. L.; Strouse, G. F. *Langmuir* **2002**, *18*, 269−276.

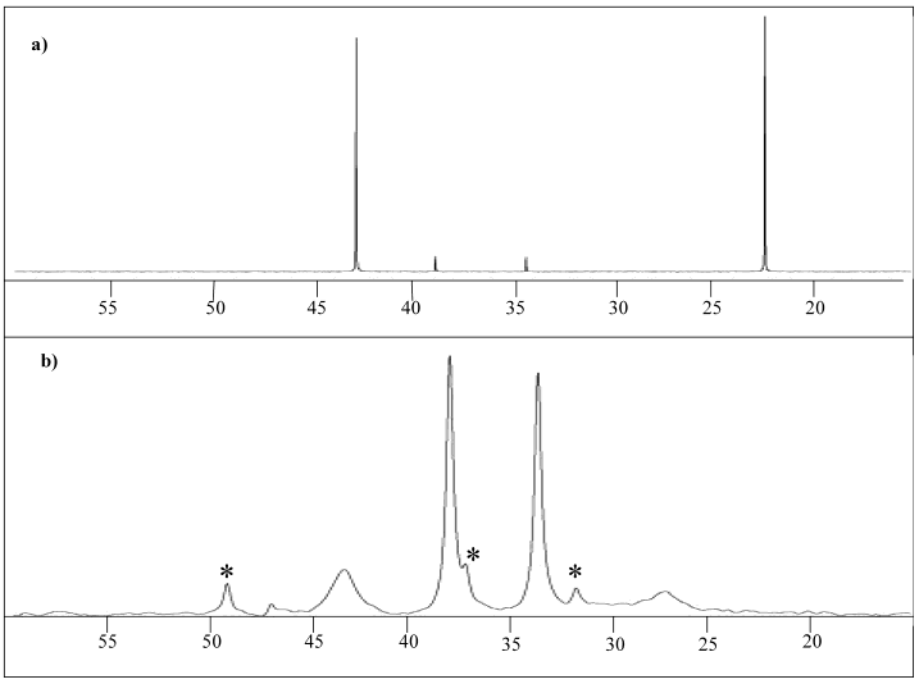

Figure 1. (a) ^{13}C NMR spectra in D_2O of aminoethanethiol (AET); (b) ^{13}C NMR spectra in D_2O of CdSe−AET. Disulfide of AET is present. The peaks observed at 34.32 and 38.89 ppm in both spectra correspond to small amounts of the disulfide of AET. Solvent impurities are labeled by an asterisk (*).

Synthesis Materials. Au nanoparticles (6.0 nm) were prepared by standard protocol in aqueous media by reduction of auric acid in the presence of sodium citrate and tannic acid.[4,47] This methodology produces gold nanoparticles with a 15% size distribution passivated by a mixture of citrate and tannic acid (Au−citrate) as shown in Figure 1 of the Supporting Information. The gold nanomaterials were precipitated in the presence of high concentrations of salts, such as sodium chloride, sodium sulfate, or sodium carbonate, to allow the gold nanoparticles to be isolated from the excess citric and tannic acid buffer solution with either a citrate/tannate (NaCl), sulfate ($NaSO_4$), or carbonate ($NaCO_3$) surface passivating layer.[47]

CdSe nanocrystals (5−6% distribution) capped with hexadecylamine (CdSe−HDA) were prepared by modification of a previously published single source lyothermal technique.[3] Briefly, 2.0 g of $[(CH_3)_4N]_4[Cd_{10}Se_4(SC_6H_5)_{16}]$ (0.574 mmol) was heated in 60 mL of hexadecylamine to 260 °C under argon.[48,50] The CdSe particle size was followed by UV−vis absorbance spectroscopy and the reaction was removed from heat when the desired nanocrystal size was reached. To collect the CdSe sample, the reaction mixture was cooled to 50 °C and 200 mL of anhydrous methanol was added to induce precipitation of the CdSe sample. The precipitate was collected by centrifuge, redissolved in a minimum amount of toluene, and reprecipitated by addition of methanol to remove excess HDA and unreacted monomer.

Size, size dispersity, and crystallinity of CdSe−HDA and Au nanoparticles were verified by optical measurements, TEM (Figure 2 in the Supporting Information), and powder X-ray diffraction analysis, as previously described.[3]

Preparation of Water Soluble CdSe (CdSe−AET). Surface ligand exchange of the hexadecylamine (HDA) passivant layer on CdSe (CdSe−HDA) by 2-aminoethanethiol (AET) was accomplished by dispersing 20 mg of CdSe−HDA in 0.5 mL of *N*,*N*-dimethylformamide with light sonication. The hydrochloride salt of AET was added (approximately 200 mg)

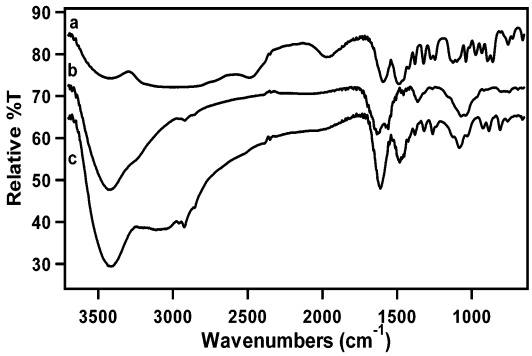

Figure 2. FT-IR spectra of (a) 2-aminoethanethiol, (b) CdSe−AET, and (c) the 1:6 Au−CdSe nanocomposite in a KBr pellet at 298 K. The spectra were recorded at 4 cm^{-1} resolution for 128 scans under a N_2 environment. Background subtraction of the FT-IR spectrum was recorded against a KBr blank.

and the suspension was heated in an oil bath at 70 °C for 5 min under N_2 with stirring. Complete dissolution of the CdSe into the DMF occurs during the ligand exchange process. The product was isolated by precipitation via the addition of methanol and the procedure was repeated to ensure complete ligand exchange was accomplished. After the final precipitation with methanol, the product was washed with methanol (3×), and dissolved in Nanopure purified water. Minimal insoluble products (<5%), if any, were removed by centrifugation. The ligand exchange yields a water-soluble CdSe−AET material with a pH of ∼5.5 when dissolved in Nanopure water. ^{13}C NMR and FTIR analysis of the water-soluble fraction indicates complete exchange of the HDA by AET within experimental analytical limits (Figures 1 and 2, respectively). Evidence for disulfide formation can be observed in the NMR as discussed in detail below. TEM analysis of these materials indicates the distribution, size, crystallinity, and shape of CdSe is unperturbed by the ligand exchange process.

Preparation of Au−CdSe Composites. Macroscopic solids on length scales up to 0.5-mm length scale can be prepared by the addition of an aqueous solution of CdSe−AET nanoparticles to a stirred aqueous solution of Au nanoparticles in a pH range of 4−6 at room temperature. For a typical

(48) Gaumet, J. J.; Strouse, G. F. *J. Am. Soc. Mass Spectrom.* **2000**, *11*, 338−344.
(49) Becerra, L. R.; Murray, C. B. et al. *J. Chem. Phys.* **1994**, *100*, 3297.
(50) Dance, I. G.; Choy, A.; Scudder, M. L. *J. Am. Chem. Soc.* **1984**, *106* (21), 6285.

synthesis, Au−citrate nanoparticles are prepared[4,47], redissolved in approximately 45 mL of water, and the pH adjusted to 4.5 with the addition of dilute acetic acid. Approximately 15 mg of CdSe−AET is dissolved in 30 mL of water and the pH is adjusted to 4.5 with dilute acetic acid. Slow addition of the CdSe sample to the Au solution produces a black solid precipitate. The product can be isolated by decanting off the supernatant and washing the precipitate several times with water and methanol. Drying under vacuum yields a hard, macroscopic composite that is insoluble in common polar and nonpolar solvents.

Systematic controls to optimize the formation of the materials were investigated by controlling the pH of the nanomaterial solutions, the mole ratios of the Au to CdSe nanoparticle solutions, and the nature of the Au surface passivating layer. No solid formation of either Au or CdSe is observed in the absence of the co-nanomaterial.

Results and Discussion

Ligand Exchange. Ligand exchange of the HDA surface passivant ligand on HDA−CdSe with 2-aminoethanethiol produces CdSe nanoparticles that can be dissolved in water to yield an optically clear solution that is stable to precipitation in the pH range from 3 to 7 for >24 h. As the pH of the CdSe−AET solution is increased to >7 the CdSe tends to aggregate and flocculate out of solution. The aggregated CdSe materials can be isolated by centrifugation and redispersed in a lower pH solution, demonstrating that the particle integrity is maintained. Addition of a pH 4−6 buffer solution (consisting of sodium citrate and tannic acid concentrations equivalent to those used for Au synthesis) to the CdSe−AET does not produce solid precipitate or noticeable changes in the optical properties, indicating that there are no significant interactions of the citrate or tannate ions with the CdSe particles. In fact, the CdSe−AET appears to be stabilized at higher buffer concentrations. Conversely, if a solution of AET is added to the gold solution alone, a precipitate of agglomerated gold nanoparticles that forms immediately cannot be redissolved in an aqueous solution. Inspection of the TEM images for this sample (not shown) indicate the Au nanomaterials have fused to form a larger amorphous material without clearly definable boundaries for individual particles.[51]

Evidence for the complete exchange of HDA for AET and the nature of the binding of terminal AET moieties to the CdSe surface in AET can be analyzed by ^{13}C NMR spectroscopy (Figure 1). Consistent with a high percentage of ligand exchange of HDA by AET on CdSe, no evidence for the ^{13}C peaks corresponding to CdSe−HDA at 32.08 ppm, 29.52−29.85, 22.83, and 14.24 ppm are present in the spectrum. The ^{13}C spectrum for CdSe−HDA is shown in the Supporting Information (Figure 3). ^{13}C NMR analysis of the hydrochloride salt of AET dissolved in D_2O yields a peak at 42.76 ppm corresponding to the carbon alpha to the nitrogen and a peak at 22.34 ppm corresponding to the carbon alpha to the sulfur (Figure 1a).[52] The peaks at 34.32 and 38.89 ppm correspond to small amounts of the disulfide present in the sample. Upon binding to the CdSe surface, the chemical shift of the carbon alpha to the nitrogen remains at 42.76 ppm but is broadened from that of free AET. The carbon alpha to the sulfur shifts downfield to 27.30 ppm and displays a broadening greater than that of the carbon alpha to the nitrogen (Figure 1b). Preferential binding of the thiolate moiety to the CdSe surface without scrambling is supported by the observation of a lack of 4 peaks or sets of carbon peaks in the NMR, expected for a system exhibiting both −S and $-NH_2$ binding of the AET at the CdSe surface. The broadening of the peaks can be attributed to a decreased T_2 relaxation time attributed to a lack of rotation upon binding to the CdSe surface.[53,54] Broadening of the NMR signals for organic amphiphiles bound to surfaces has previously been observed for both CdSe and Au nanomaterials in earlier studies.[49,54] The greater broadening and the large shift of the carbon alpha to the sulfur suggest preferential R−S binding to the CdSe surface. Binding of the sulfur to the CdSe instead of the ammonium functionality is further supported by the observation of the water solubility, which is predicted for a terminal ammonium group interacting with water. Although the NMR data do not disprove R−SH binding as a possibility, it is strongly suggestive of only thiol binding dominating the AET interaction with the CdSe surface.

In the ^{13}C spectrum, additional peaks arising from formation of the disulfide of AET at 34.32 and 38.89 ppm are present in both spectra, possibly due to instability of the short chain ligand on the surface or photooxidation of AET as has been reported for thiols on CdSe surfaces.[55] Impurities due to DMF at 31.79 and 38.13 ppm and methanol at 49.29 ppm are also identified in the spectra arising from the recapping protocol. The peaks corresponding to the disulfide, DMF, and methanol are artificially broadened due to data processing from the line-broadening of 50 Hz in order to enhance the broadened signals of the bound AET.

Verification of terminal amine/ammonium functionalities in the AET−CdSe sample can be gained by inspection of the FT-IR data for AET−CdSe (Figure 2, Table 1). The lack of a peak in CdSe−AET at 2490 cm^{-1} for the RS−H confirms the loss of the free thiol upon surface binding. In CdSe−AET, the peak observed at 3395 cm^{-1} is assignable to an N−H stretch. The peaks at 1480 cm^{-1} and 1600 cm^{-1} are assignable to symmetric and asymmetric NH bends.[52] The peak positions for the NH modes in comparison to the free hydrochloride salt of AET are consistent with an ammonium terminal functionality as observed in the ^{13}C NMR spectra. The small shift in frequency for the symmetric stretch in comparison to the hydrochloride salt of AET probably arises from changes in the NH_2/NH_3 ratio upon binding to the CdSe surface, due to hydrogen bonding.

Composite Composition. The 3-D macroscopic composite is formed from mixing aqueous Au−citrate and AET−CdSe at room temperature. This leads to the formation of a dark particulate matter, whose solid-state absorption spectrum (measured in KBr) is composed of contributions from both the Au and CdSe nanocomponents, allowing analysis of the optical absorption spec-

(51) Cumberland, S. L.; Strouse, G. F. unpublished results.

(52) Silverstein, R. M.; Bassler, G. C.; Morrill, T. C. *Spectrometric Identification of Organic Compounds*, 5th ed.; Wiley: New York, 1991.

(53) Sachleben, J. R.; Wooten, E. W., et al. *Chem. Phys. Lett.* **1992**, *198* (5), 431.

(54) Pan, C.; Pelzer, K.; Philippot, K.; Chaudret, B.; Dassenoy, F.; Lecante, P.; Casanove, M.-J. *J. Am. Chem. Soc.* **2001**, *123*, 7584.

(55) Aldana, J.; Wang, A. Y.; Peng, X. *J. Am. Chem. Soc.* **2001**, *123* (36), 8844−8850.

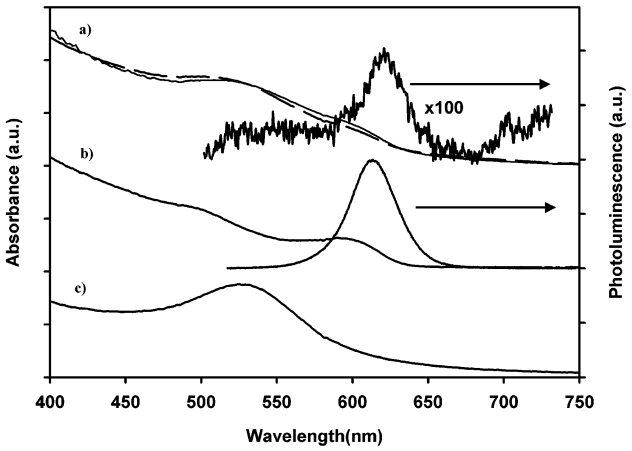

Figure 3. (a) Solid-state absorbance spectra (solid line), absorption profile fit (dashed line), and emission spectra (λ_{ex} = 488 nm, 2 mW) for the 1:6 Au−CdSe nanocomposite in a KBr pellet at 298 K. (b) Solution phase absorbance (solid line) and emission spectra (λ_{ex} = 488 nm, 2 mW) for CdSe−AET in H_2O at 298 K. (c)Solution-phase absorbance spectra (solid line) for 6.0 nm Au−TA in H_2O at 298 K. The theoretical fit of the absorption profile (dashed line) in Figure 3a was fit using a weighted combination of the solution phase CdSe and Au spectra in Figure 3b and 3c respectively, as well as the inclusion of a scattering profile for the KBr solid pellet absorbance.

Table 1. Room-Temperature FT-IR Assignments for KBr Pellets of AET, CdSe−AET, Au−CdSe, Octylamine, and Au−Octylamine

compound	wavenumbers (cm^{-1})	assignment
AET	3425	NH_3^+ (N−H) stretch
	1595	NH_3^+ (N−H) bend (asym)
	1490	NH_3^+ (N−H) bend (sym)
	1100	C−N stretch (νC−N)
	2490	S−H stretch
CdSe−AET	3395	NH_3^+ (N−H) stretch
	1600	NH_3^+ (N−H) bend (asym)
	1480	NH_3^+ (N−H) bend (sym)
	1620	N−H bend (δNH_2)
	1068	C−N stretch (νC−N)
	810	N−H wag
Au−CdSe	3286	N−H stretch (asym)
	3148	N−H stretch (sym)
	1550	N−H bend (δNH_2)
	1050	C−N stretch (νC−N)
	757	N−H wag
octylamine	3372	N−H stretch (asym)
	3295	N−H stretch (sym)
	1610	N−H bend (δNH_2)
	1073	C−N stretch (νC−N)
	796	N−H wag
Au−octylamine	3286	N−H stretch (asym)
	3221	N−H stretch (sym)
	1556	N−H bend (δNH_2)
	1037	C−N stretch (νC−N)
	800	N−H wag

trum to gain insight into the composition of the material (Figure 3). Further information can be gained by inspection of the electron microscopy and energy-dispersive X-ray analyses in Figures 4−8. It is interesting to note that the reaction proceeds to the same final product regardless of the Au pasivating ligand, Au−citrate, Au−carbonate, or Au−sulfate, or buffer choice. The differences in the reaction are in reaction rates and in final composite dimensions not composition. For simplicity, the discussion will focus on the Au−citrate reaction with CdSe−AET.

Figure 3 provides direct evidence of an interconnected 3-dimensional composite of Au and CdSe nanomaterials. The absorption spectra for the solid composition exhibits evidence for complexation, with absorption features assignable to both the CdSe exciton absorption at 610 nm and the Au SPR band at 520 nm. Inspection of the absorption spectrum in Figure 3 allows an estimate of the Au−CdSe ratio in the final macroscopic assembly if we assume noninteracting nanomaterials, as described in the Experimental Section, eq 1. This allows the mol:mol ratios of the CdSe and Au nanoparticles to be extracted by substitution of the Beer−Lambert law in eq 1, $A(\lambda) = \epsilon(\lambda)b[A]$

$$A_{\text{Composite}}(\lambda) = \epsilon_{\text{CdSe}}(\lambda)[\text{CdSe}] + \epsilon_{\text{Au}}(\lambda)[\text{Au}] + f_{\text{scat}}(\lambda) \quad (2)$$

This allows a qualitative estimate of the mol:mol ratio of CdSe to Au, [CdSe]/[Au] in the composite to be solved by employing a nonlinear statistical fitting routine using a Levenberg−Marquadt algorithm. The fit parameters consisted of, in addition to [CdSe] and [Au], an arbitrary absorbance baseline and a scaling factor for the scattered light. Fitting of the absorption data yields a value for the [CdSe]/[Au] ratio of ∼6−7 CdSe to 1 Au in the formed composite.

Although the fit reproduces many features in the composite, as shown in Figure 3, there is a noticeable deviation which must arise from the interaction between the constituents. Comparison of the Au−citrate spectrum and the Au−AET−CdSe composite spectrum reveals an apparent shift and broadening of the SPR band for Au to lower frequency upon formation of the assembled material. Ligand-induced changes in the SPR band for Au are well documented in the literature.[56] The distance-dependent coupling of the surface plasmons in colloidal gold aggregates can induce a bathochromic shift in the surface plasmon band. In fact, the position and breadth of the observed Au SPR band in the composite is consistent with observations of the position and width of the SPR band of Au passivated with octylamine.[57] This supports a model in which the thiol is bound to the CdSe surface and the amine interacts with the Au surface to form a Au−NH_2R coordination. A loss of contributions to the absorption spectrum from tannic acid on Au at higher energy is also noted, indicating displacement of the citrate and tannic acid from the Au surface upon formation of the assembly. Consistent with the picture of discrete ligands connecting Au and CdSe particles, there is no optical evidence for Au agglomeration, which is characterized by a broad absorption band from 520 to 685 nm.[58−60]

Further support of an interconnected network composed of Au and CdSe can be gained by inspection of the emission properties of the composite to a drop-cast film of CdSe−AET, and a mixture of CdSe−HDA and Au−DDT. Excitation into the exciton transition for the

(56) Schmelz, O.; Mews, A.; Basché, T.; Herrmann, A.; Müllen, K. *Langmuir* **2001**, *17* (9), 2861−2865.
(57) Cumberland, S. L. Ph.D. Thesis, University of California at Santa Barbara, Oct. 2001.
(58) Mie, G. *Ann. Phys.* **1908**, *25*, 277.
(59) Lin, X. M.; Sorensen, C. M.; Klabunde, K. J. *Chem. Mater.* **1999**, *11*, 198.
(60) Kumar, A.; Mandale, A. B.; Sastry, M. *Langmuir* **2000**, *16* (24), 9299−9302.

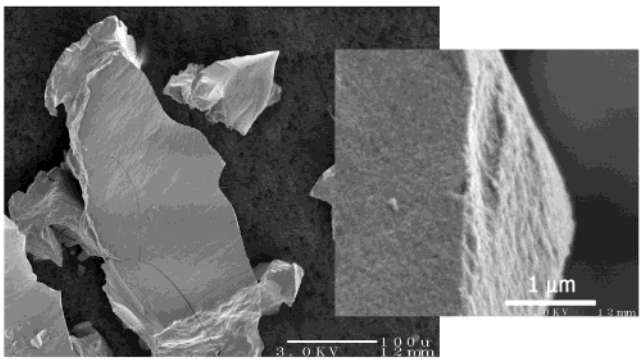

Figure 4. SEM backscattered image of a mechanically fractured macroscopic 1:6 Au−CdSe nanocomposite at 10 000 magnification (3 kV) on a carbon substrate (100-μm scale bar). Inset represents a magnification (3 kV) of a fractured edge of the CdSe−Au nanocomposite on the Si substrate (100-μm scale bar).

CdSe at 488 nm leads to a lack of emission from the composite. In contrast, in self-assembled structures in which the Au and CdSe nanomaterials are stoichiometrically deposited on a flat substrate by evaporative deposition from an organic phase, localized regions of CdSe emission are observed. The lack of emission in the composite arises from rapid quenching of the CdSe by photoinduced electron injection or energy transfer to the Au nanoparticle.

Imaging of the Au−CdSe composite by scanning electron microscopy (SEM) and transmission electron microscopy (TEM) provides further insight into the compositional and structural morphology of the composite (Figures 4−8). SEM analysis of the collected product shows submicrometer-scale structures are generated, which at higher magnification exhibits a granular morphology (Figure 4). The granular morphology arises from the conformation of closely packed spheres of nanoparticles in the assembly. At high magnification, individual nanomaterials cannot be observed in the composite due to distortion of the SEM image arising from charging of the semiconducting nanoparticles in the matrix.

Scanning electron microscopy energy-dispersive X-ray analysis (SEM−EDX) of the nanocomposite provides insight into the uniformity of the composite. Inspection of the SEM−EDX (Figure 5) data allows a direct measure of the average composition of the 3-D Au−AET−CdSe composite formed at pH 4.5 by imaging the composition in the 500 × 500 nm field of view of the SEM at low magnification. The EDX data reveals a ∼1:6 composition ratio of Au to CdSe nanomaterials. This is confirmed over 6 sample regions in the SEM and correlates with the experimentally measured mole ratio for Au to CdSe in the optical absorption spectrum. Intriguingly, the final composition is 1:6 under conditions of either 6 molar equivalents of CdSe to 1 molar equivalent of Au or 60 molar equivalents CdSe to 1 molar equivalent of Au (Table 2). The observation of an invariant ratio of Au to CdSe in both the optical absorption and SEM−EDX data suggests the mechanism for formation is thermodynamic driven by a coordination event of the AET to the Au surface, rather than a kinetic structure that is largely amorphous, assembled by only soft sphere packing forces. The mechanism is discussed in detail in the following section.

Table 2. Average Composition for a 500 × 500 nm Region of a Macroscopic Sample of the Au−AET−CdSe Composites Formed at pH 4.5 as Shown by SEM−EDX Analysis[a]

reaction condition	initial mole ratios		observed weight %		
	Au	CdSe	Au	Cd	Se
calculated[b]	1	6	36.2	34.6	29.2
pH 4.5	1	6	34.3	37.7	28.0
pH 4.5	1	60	34.7	37.8	27.5

[a] The measurement was conducted on a Si substrate in backscattering mode at 3 kV and calibrated against a Cu powder standard. [b] Calculated weight percentages are based on the predicted weight % composition for a 1:6 mole ratio of Au to CdSe, which is composed of 6667 Au atoms in the 6-nm Au particle and 2022 CdSe molecules in a 6-nm CdSe particle. The AET was assumed to account for 20% of the sample mass.

Whereas SEM imaging provides insight into the composite composition, TEM imaging and selected area electron diffraction (SAED) in the TEM provides information into the nature of the individual component interactions within the assembly (Figure 6). Because of the thickness of the composite, only the edge of the fractured composite can be directly imaged. It should be noted that analysis of the edge would provide only indirect support of the bulk of the material, because the edge is formed by fracturing the composite under mechanical stress. Figure 6a shows a TEM image of the Au−CdSe assembly several micrometers in length composed of 6.0-nm Au and 6.0-nm CdSe nanoparticles. In the TEM image the Au nanomaterials are readily identifiable (gray particles), but CdSe can be identified at high magnification only by its characteristic fringe pattern (Figure 6c). Comparison of the initial Au and CdSe nanomaterial size distributions to the distributions of the particles in the composite indicates the exclusion of poorly formed and large Au particles from the assembly. The TEM image illustrates that the nanomaterials exist as closely packed spherical particles which exhibit well-defined edges, indicating the composite is composed of individual nanoparticles without evidence of material alloying.

Figure 7 shows the SAED pattern for the Au−CdSe composite with a corresponding intensity distribution curve contrasted against SAED curves for individual Au and CdSe nanoparticles. Because of the limited distances observable in the SAED pattern, the Debye−Scherrer rings observed in the SAED pattern for the Au−CdSe composite originate only from contributions assignable to Bragg reflections for the individual Au and CdSe sub-components, rather than reflecting long-range crystallinity of the entire composite. The rings correspond to lengths of 2.877, 2.557, 2.332, 2.1666, 1.999, 1.568, and 1.333 Å. Peak position assignments can be made by comparison against SAED and powder X-ray diffraction patterns for Au and CdSe nanoparticles surface-stabilized with long chain alkanes. The rings at 2.557 and 2.166 Å are solely from the Au nanoparticles and correspond to the ⟨111⟩ and ⟨200⟩ planes of the gold nanoparticles, respectively. The rings at 2.877, 2.332, and 1.999 Å correspond to lattice fringes assigned in the CdSe spectrum. The ring at 2.877 corresponds to the ⟨002⟩ plane of the CdSe but is broadened by contributions from the ⟨100⟩ and ⟨101⟩ planes. The rings

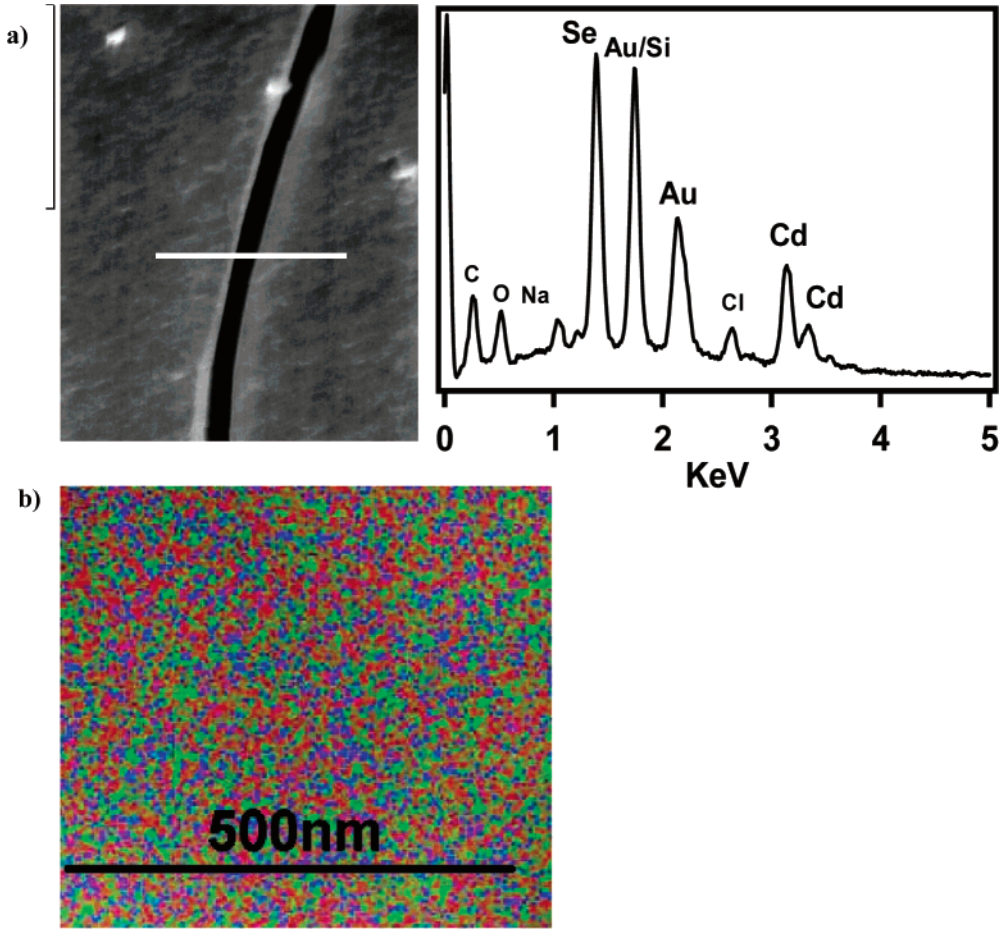

Figure 5. (a) SEM backscattered image (3 kV) and SEM−EDX intensity patterns for a selected region of the 1:6 Au−CdSe nanocomposite on a Si wafer support, and the average elemental composition map over the 1-μm line scan; and (b) SEM−EDX image map of a 500 × 500 nm region indicating the areas of Au (blue), Cd (green), and Se (red) measured on the sample imaged in Figure 5a.

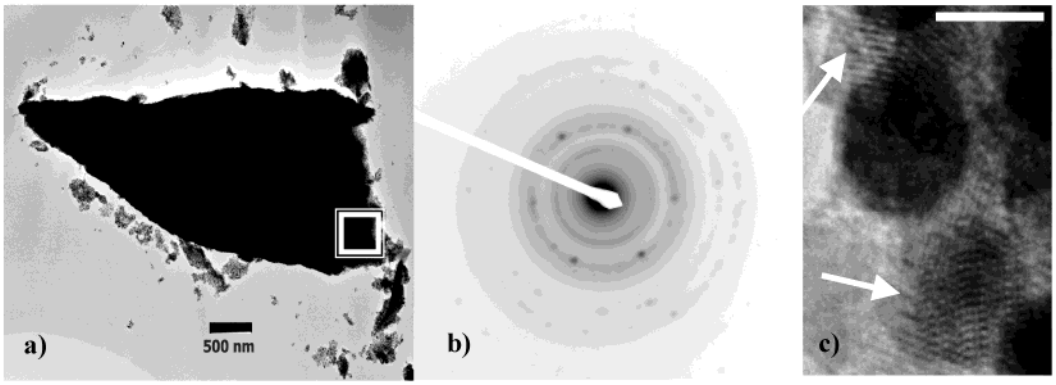

Figure 6. (a) Bright field TEM image (13 000× magnification, 200 kV) on a Cu grid coated with 5 nm of holey carbon for the 1:6 Au−CdSe nanocomposite material (500-nm scale bar). (b) Selected-area electron diffraction pattern (200 kV at 83.0 cm camera length) obtained from a 50-nm region of the composite (square on image (a) indicates region of SAED image), and (c) higher magnification (210 000× magnification, 200 kV, 5-nm scale bar) of a fractured edge of the macroscopic composite showing individual 6.0-nm gold and 6.0-nm CdSe nanoparticles. The Au nanoparticles in the image are identifiable as the gray spheres, whereas the CdSe are indicated by arrows and are identifiable by the characteristic fringe pattern for a wurtzite nanocrystal of CdSe.

at 2.332 and 1.999 Å correspond to the ⟨110⟩ and ⟨112⟩ planes of the CdSe, respectively, with the greatest contribution from the ⟨110⟩ plane. The rings at 1.568 and 1.333 Å are a combination of peaks from both the CdSe and Au, but, based on intensity arguments, can be assigned to the ⟨220⟩ and ⟨311⟩ planes of the gold nanoparticles, respectively.[22,61,62]

Inspection of the tilt-dependent SAED patterns (Figure 8) reveals the electron diffraction image has contributions from both diffraction rings, arising from the isotropic (random) ordering of the nanomaterials within the composite, and intense diffraction spots, which are assignable to anisotropic (discrete) ordering of the nanomaterials within the composite structure. On the

(61) Revaprasadu, N.; Malik, M. A.; O'Brien, P.; Wakefield, G. *Chem. Commun.* **1999**, 1573.
(62) Akamatsu, K.; Deki, S. *J. Colloid Interface Sci.* **1999**, *214*, 353.

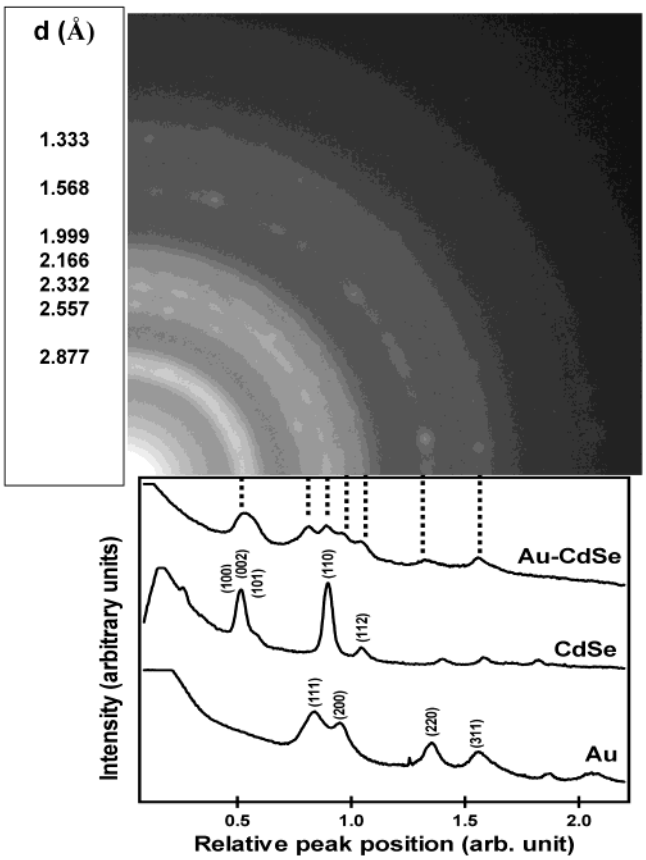

Figure 7. TEM selected-area electron diffraction pattern (SAED) (200 kV, 83.0 cm camera length) for a 50-nm region of the Au−CdSe composite indicated in Figure 6. The SAED ring patterns are scaled to *d*-spacing by calculation of the TEM image for the given camera length. Included in the image is a comparison of the SAED intensity distribution curve for individual 6.0-nm gold and 6.0-nm CdSe nanoparticles, as well as the Au−CdSe composite.

basis of the position of the observed hexagonal pattern in the SAED-tilt experiment, the pattern arises from contributions for the preferred packing orientations of the CdSe crystallite faces within the final composite relative to the plane defined by the electron beam. This is consistent with the enhanced intensity of the ⟨110⟩ plane for the CdSe in the SAED image. Observations of similar SAED spot patterns in self-assembled nanocrystal assemblies have been interpreted as arising from preferential ordering of crystalline nanomaterial lattice planes.[29,42,63−65]

The observation of the hexagonal pattern over several lattice planes in the SAED image suggests that longer range ordering of the nanomaterials may arise in these materials than was predicted. Although evidence of nanomaterial ordering is observed in the composite, this can be interpreted only in terms of local ordering or polycrystallinity in the structure due to the combination of rings and diffraction patterns in the tilt-dependent SAED images.

Influence of Reaction Conditions on Composition. The effect of the pH on the final composite composition can be analyzed by inspection of pH-dependent data. There are 3 regimes observed in the pH-dependent analysis. At pH >6, no precipitation or changes in the absorption spectra are observed. TEM analysis of the solution evaporated onto a TEM grid indicates a pattern of randomly oriented Au and CdSe nanomaterials. In the pH range 3.0−4.5 an immediate reaction is observed with formation of a precipitate on the order of ∼1 micrometer. TEM analysis of the composite structures indicates a 1:6 ratio of Au−CdSe for disordered assemblies, regardless of initial reaction stoichiometry in the EDX experiment, yet only ring patterns are observed in the TEM−SAED imaging. In the pH range 5.0−6.0, well-formed 1:6 structures are observed giving rise to the observed SAED−TEM hexagonal pattern shown in Figure 8 arising from the preferential ordering of the subcomponent CdSe nanomaterials in the composite (Figure 7).

Mechanism for Composite Formation. Several mechanisms for the formation of the composite structure are possible including self-assembly, electrostatic attraction, ligand exchange, or coordination-induced coupling. The formation of the Au−CdSe composite appears to be driven by acid−base equilibria based on the pH and mole ratio dependence for the assembly. The observation of a ∼1:6 mole ratio for Au to CdSe in the absorption spectrum and EDX-SEM can be interpreted as arising from a statistical population in the ensemble, in which the final product should reflect the initial stoichiometry of the reaction, or a controlled coupling of the particles via a thermodynamically driven self-assembly step in which the final composition is independent of the initial stoichiometry. This supports a thermodynamically controlled reaction mechanism modulated by the formation of the Au−NH_2−R−S−CdSe coordination bond as proposed in Figure 9. The mechanism represents the proposed reaction of Au−citrate with CdSe−AET; however, it is believed a similar mechanism applies to the reaction with Au−carbonate and Au−sulfate, which produce identical composite structures. Displacement of the carboxylate (or sulfate, carbonate) stabilizing functionality on the Au surface leads to the formation of a composite modulated by a proton transfer from the ammonium functional group of the AET to the citrate passivating ligand. Buffering of the solution controls the rate of exchange for the ammonium proton with the citrate group on the Au nanoparticles, providing a driving force for the amine functionality to bind the Au surface while prohibiting the reverse exchange of the proton back to the amine group. The formation of the bond is believed to be driven by the availability of the lone pair of electrons of the amine to interact with the gold surface. A similar reaction mechanism has been proposed for displacement of citrate ions from gold surfaces by alkylamines during surface ligand exchange.[66−68]

Direct self-assembly appears to be a minor contributor to the assembly of the composite. Nontemplated, evaporatively self-assembled structures prepared by the

(63) Harfenist, S. A.; Wang, Z. L.; Alvarez, M. M.; Vezmar, I.; Whetten, R. L. *J. Phys. Chem.* **1996**, *100*, 13904.
(64) Murray, C. B.; Kagan, C. R.; Bawendi, M. G. *Science* **1995**, *270*, 1335.
(65) Wang, Z. L.; Harfenist, S. A.; Vezmar, I.; Whetten, R. L.; Bentley, J.; Evans, N. D.; Alexander, K. B. *Adv. Mater.* **1998**, *10*, 808.
(66) Sato, T.; Hasko, D. G.; Ahmed, H. *J. Vacuum Sci. Technol. B* **1997**, *15*, 45.
(67) Lyon, L. A.; Pena, D. J.; Natan, M. J. *J. Phys. Chem. B* **1999**, *103*, 5826.
(68) Larson, I.; Chan, D. Y. C.; Drummond, C. J.; Grieser, F. *Langmuir* **1997**, *13*, 2429.

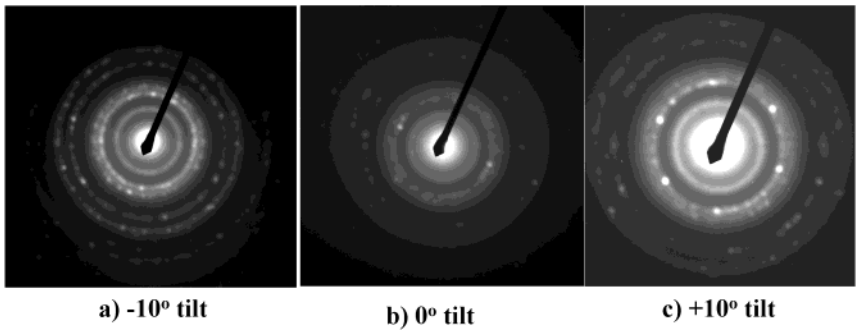

Figure 8. Selected-area electron diffraction (SAED) tilt dependent pattern over a 50-nm region (200 kV, 83.0 cm camera length) of the composite at (a) −10°, (b) 0°, and (c) +10° illustrating the appearance of a regular pattern for the CdSe nanomaterials in the Au−CdSe composite indicating preferential ordering of the nanomaterials in the composite.

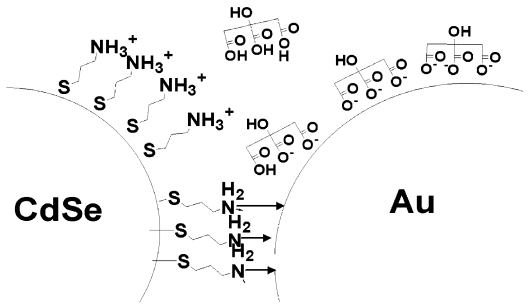

Figure 9. Proposed reaction mechanism for the formation of the 1:6 Au−CdSe composite for a CdSe−AET and Au−TA composite.

intimate mixing of a toluene solution with a 1:1 mole ratio of 6.0-nm CdSe capped with hexadecylamine and 6.0-nm Au capped with hexadecanethiol produces only phase-segregated materials with a distribution reflecting the stoichiometry of the reactants (Figure 10). Electrostatic and hydrogen bonding contributions are also believed to be negligible contributors to the assembly based on FT-IR analysis.[38] The lack of evidence for citric acid, tannic acids or salt, (or sulfate, carbonate) incorporation into the structure or IR modes assignable to RNH_3^+ (Figure 2) is consistent with the lack of electrostatics dominating the assembly mechanism. Contributions from ligand exchange to assembly may play a role in the final structure, but can be eliminated as a primary driving force for the composite formation based on IR analysis of the starting materials and final product, as discussed earlier. Although these mechanisms are minor contributors to the final assembly, it is expected they still play a role in the initial formation of the composite.

The proposed mechanism in Figure 9 is consistent with coordination events controlling the formation of the composite and the negligible contributions of electrostatic, hydrophobic, or hydrogen bonding contributions in these composites. Assuming the above mechanism, the observation of a concentration-independent formation of a 1:6 composite of Au−CdSe is predicted for control of assembly initiated by formation of a $Au-NH_2$ bond. The 1:6 ratio is believed to arise from an AET−CdSe dominated acid−base reaction, and the desire to closely pack the spherical particles in the final structure. The arrangement is analogous to a CCP structure in ionic solids. This suggests that long-range order in these composites may be achievable under appropriate temperature, reaction mixing rates, and pH.

The proposed mechanism can be supported by comparison of the FTIR spectra of free AET, CdSe−AET, and the final Au−CdSe product (Figure 2). Analysis of the Au−CdSe FT-IR spectra indicates a loss of the ν_{COO^-} at 1710 cm^{-1} and the $\nu_{NH_3^+}$ mode at 1485 cm^{-1}. The ν_{NH_2} modes at 3400 cm^{-1} shift to lower frequency in the 3100−3300 cm^{-1} region and decrease in intensity, as expected for the formation of a metal−amine bond.[69,70] Similar shifts are observed for octylamine monolayers on gold surfaces, with a shift in the ν_{NH_2} modes of octylamine from 3292 and 3370 cm^{-1} to 3220 and 3286 cm^{-1}, respectively, upon binding to gold (Table 1). The shift to lower frequency for ν_{NH_2} in the Au−CdSe product

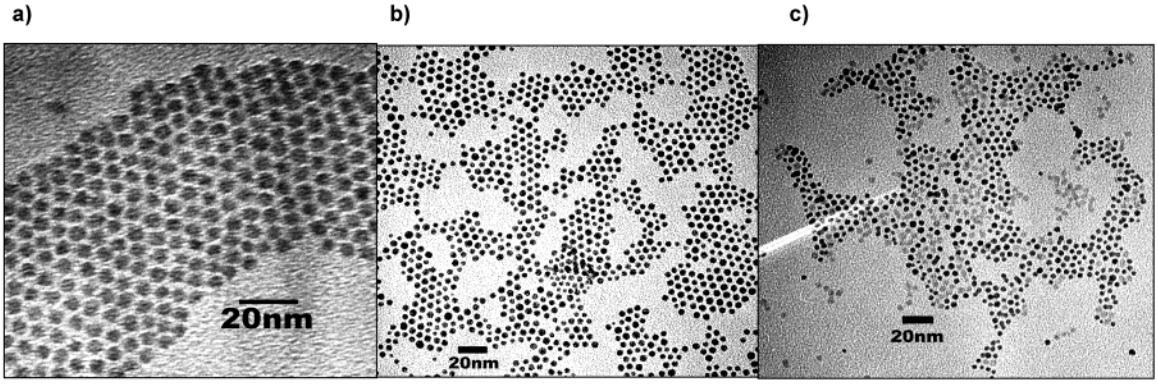

Figure 10. Bright field TEM image for individual nanoparticles evaporatively assembled on a Cu grid coated with 5 nm of holey carbon from slow evaporation of toluene for (a) 6.0-nm Au (200 kV, 340 000× magnification), (b) 6.0-nm CdSe (200 kV, 250 000× magnification), and (c) a 1:1 mixture of 6.0-nm Au (hexadecylthiol capped) and 6.0-nm CdSe (hexadecylamine capped) in toluene (200 kV, 100 000× magnification). The scale bar is 20 nm.

is consistent with a metal−NH_2 interaction and loss of the ammonium proton.

Further evidence for formation of Au−NH_2RS−CdSe bonds in the composite is provided in the IR data for the δ N−H bending modes in the 1500−1600 cm^{-1} region. Upon formation of the free-standing composite, the δ N−H bending mode assignable to ammonium disappear, and the amine bending vibration shifts to 1550 cm^{-1} consistent with formation of a Au−NH_2R bond. The bond formation is further corroborated by inspection of the N−H wagging mode observed at 810 cm^{-1} for the free amine/ammonium group in CdSe−AET which shifts to 800 cm^{-1} in the composite, and the shift in the C−N stretching mode from 1100 cm^{-1} in the free amine/ammonium group to the bound Au−NH_2R confirmation at 1050 cm^{-1}. Similar changes in intensity and frequency of these bands relative to the free amines have been reported for gold functionalized with alkanethiols and alkylamines.[27,70,71]

Conclusion

Control over the 3-dimensional assembly of these nanoscale composites can be controlled by thermodynamic equilibria reactions and kinetic assembly; in essence a competition between the thermodynamic interaction potentials for steric, van der Waals, and covalent energy terms arising from coordination of a ligand to a nanomaterial surface. The magnitude of the covalent energy term contribution can be manipulated by the choice of the terminal functional group on the passivating layer of one nanomaterial and the energetics of coordination on the surface of a second nanomaterial. By application of acid/base equilibrium control, assemblies composed of a 1:6 Au to CdSe ratio of two different nanomaterials can be achieved. This is confirmed by both optical absorption and electron microscopy analysis. Further analysis of this mechanism, by changes in chain lengths, terminal functionalities, and nanomaterials, are underway.

Acknowledgment. We thank M. A. Hines and P. M. Guyot-Sionnest (Univ. Chicago) for assistance in developing the technology for preparation of nanomaterials. Research supported by the National Science Foundation, Division of Materials Research CAREER Program under contract DMR-9875940. S.L.C. acknowledges a UC-GOF Fellowship at UCSB for financial support. M.G.B. thanks Mitsubishi Chemical Center for Advanced Materials at UCSB for financial support.

Supporting Information Available: Supplemental figures showing representative TEM images of the 6-nm Au−citrate nanomaterials (Supplemental Figure 1) and 6-nm CdSe (Supplemental Figure 2), and ^{13}C NMR spectra of 6.0-nm CdSe−HDA and HDA, where HDA is *n*-hexadecylamine (Supplemental Figure 3). These materials are available free of charge via the Internet at http:/pubs.acs.org.

(69) Leff, D. V.; Brandt, L.; Heath, J. R. *Langmuir* **1996**, *12*, 4723.
(70) Bharathi, S.; Fishelson, N.; Lev, O. *Langmuir* **1999**, *15*, 1929.
(71) Tian, F.; Klabunde, K. J. *New J. Chem.* **1998**, *22*, 1275.

CM010588O